Self-archived version:
M. Ciofalo, M. Di Liberto, L. Gurreri, M. La Cerva, L. Scelsi, G. Micale, *Mass transfer in ducts with transpiring walls*, International Journal of Heat and Mass Transfer, 132 (2019) 1074–1086, https://doi.org/10.1016/j.ijheatmasstransfer.2018.12.059

Mass transfer in ducts with transpiring walls

M. Ciofalo*, M. Di Liberto, L. Gurreri, M. La Cerva, L. Scelsi, G. Micale

Dipartimento dell'Innovazione Industriale e Digitale, Università di Palermo, Italy

*Corresponding author; email michele.ciofalo@unipa.it

Abstract. The problem of mass transfer in ducts with transpiring walls is analysed: the concepts of "solvent" and "solute" fluxes are introduced, all possible sign combinations for these fluxes are considered, and relevant examples from membrane processes such as electrodialysis, reverse osmosis and filtration are identified. Besides the dimensionless numbers commonly defined in studying flow and mass transfer problems, new dimensionless quantities appropriate to transpiration problems are introduced, and their limiting values, associated with "drying", "desalting" and "saturation" conditions, are identified. A simple model predicting the Sherwood number Sh under all possible flux sign combinations is derived from the single simplifying assumption that concentration profiles remain self-similar (so that the Sherwood number based on diffusion only remains unchanged) also under transpiration conditions. The simple model provides not only local values of Sh, but also its axial profiles. Predictions are validated against fully predictive CFD results, not based on the above simplifying assumption, and a good agreement is demonstrated provided the transpiration rate complies with certain limitations, depending on the Schmidt number.

Key words: Mass Transfer; Transpiring Wall; Sherwood Number; Computational Fluid Dynamics; Parallel Flow

1. General aspects of wall transpiration

A *transpiring* wall is a surface, adjacent to a boundary layer or duct flow, through which fluid passes either into the main stream (*injection*, or *blowing*) or out of it (*suction*). It is generally understood that the transpiration areal flow rate is small compared to the main areal flow rate. Transpiration may occur either through a porous (permeable) wall or through physically distinct orifices in an otherwise impermeable wall (Figure 1).

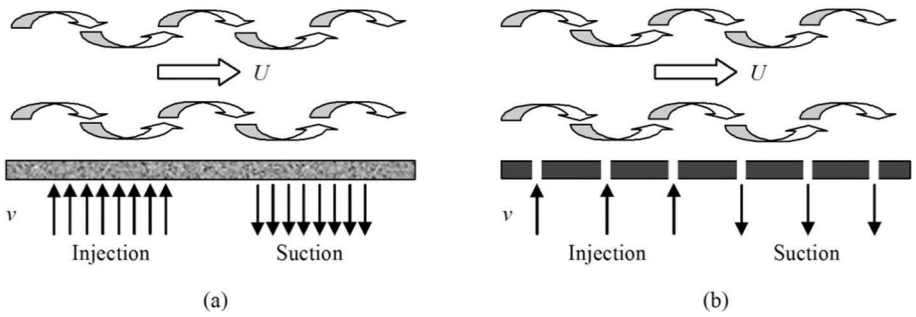

Figure 1. Transpiring walls with either injection (blowing) or suction: (a) porous; (b) perforated.

Transpiration may modify the distribution of velocity and, if present, temperature or other scalars, and thus affect momentum, heat and mass transfer between the main fluid stream and the wall. Therefore, it has been studied for a long time, either experimentally or by analytical and numerical techniques, in connection with such problems as:

- boundary layer control, e.g. delaying or avoiding transition to turbulence [1, 2];
- transpiration cooling, i.e. protecting solid surfaces (such as turbine blades [3] or re-entry vehicles [4]) from a high-temperature gas flow by blowing;
- prevention of scaling in processes like supercritical water oxidation [5].

Also phenomena of evaporation / condensation from / to a wall-adjacent liquid film (Figure 2), as may occur, for example, in nuclear reactor containment cooling problems [6], exhibit strong analogies with transpiration (blowing / suction) phenomena, so that their prediction can benefit from the modelling efforts devoted to these latter.

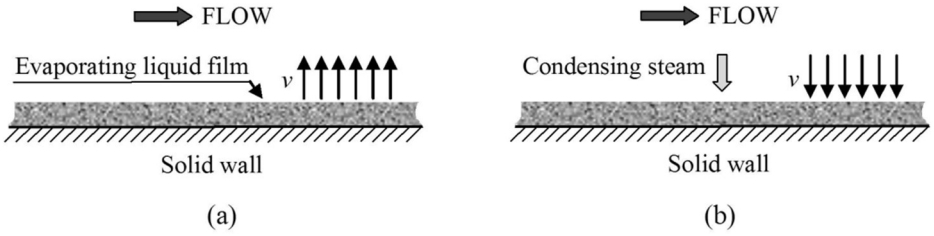

Figure 2. Evaporating (a) or condensing (b) liquid films, approximating blowing / suction conditions.

From these studies, the following synthetic conclusions can be drawn:

a) In laminar boundary layers, suction delays transition to turbulence [2].
b) Both in laminar and in turbulent boundary layers, blowing reduces friction and fluid-to-wall heat transfer, while suction increases them [1, 7]. For example, Figure 3 (drawn from data in [1]) reports the Stanton number St_x (based on the distance x from the leading edge) in a flat plate boundary layer as a function of the blowing factor v/U_∞ (positive for injection, negative for suction) at different values of the Reynolds number Re_x. Note that St_x tends to zero for $v/U_\infty \to \infty$ (large injection rate), while it tends to $-v/U_\infty$ (and thus diverges) for $v/U_\infty \to -\infty$ (large suction rate). Re_x has only a minor influence.
c) In transpired boundary layers, a similar behaviour is exhibited by the Stanton number and the friction coefficient, so that the Reynolds analogy ($St_x = C_f/2$) continues to hold.

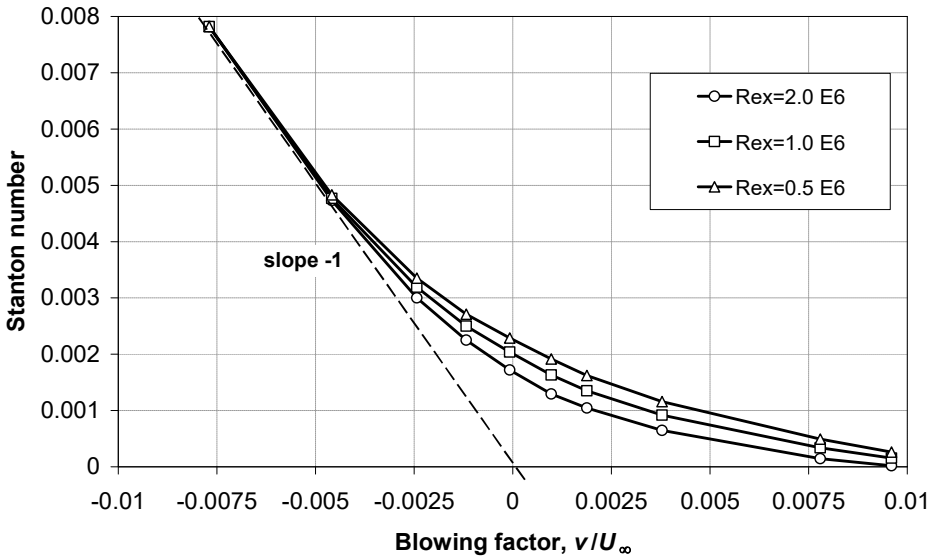

Figure 3. *x*-Stanton number as a function of the blowing factor for three different values of the *x*-Reynolds number (from results in Kays and Moffat [1]).

Most transpiration problems studied in the literature regard heat or momentum transfer. The present work focuses on the influence of wall transpiration on *mass* transfer. Note that:

a) Wall transpiration is itself a process of mass transfer between a wall and a fluid stream, since the transpiration flow carries its own mass. However, by "mass transfer" we denote here a separate process involving the transfer of a massive species other than the carrying fluid, i.e. a component dispersed in the fluid itself either at molecular/ionic scale (such as salt) or at a coarser scale (such as small solid particles). For the sake of simplicity, in all these cases we will

call the carrier fluid the "solvent" and the dispersed component the "solute" (for brevity, inverted commas will be omitted in the following). Examples include such processes as electrodialysis, reverse osmosis or filtration, involving selective membranes.

b) A well-known analogy exists between heat and mass transfer. However, mass transfer exhibits some peculiar characteristics of its own. First, the transfer of a solute, unlike that of heat, affects the mass balance of the solution. Second, solutes are generally characterized by Schmidt numbers (10^2-10^3) much higher than the Prandtl number of most fluids (with the exception of oils and other highly viscous media). Finally, selective barriers exist that can prevent the passage of the solute along with the solvent through a wall, whereas this is hardly possible for heat.

2. Mass transfer with transpiring walls

2.1 Diffusive and convective mass fluxes

In the presence of transpiration, the total solute mass flux j_S (in kg m^{-2} s^{-1}) can be expressed as the sum of a diffusive component j_{diff} and a convective component j_{conv}:

$$j_S = j_{diff} + j_{conv} = -\rho D(\partial C/\partial y)_w + \rho v C_w \tag{1}$$

in which ρ is the solution density (in kg m^{-3}), D is the solute diffusivity (in m^2 s^{-1}), C is the solute concentration (expressed as a mass fraction, e.g. as kg kg^{-1}), the suffix w denotes the transpiring wall, y is the direction normal to it and into the fluid, v is the transpiration velocity into the fluid, and j_S is positive if directed from the wall to the fluid.

The total mass transfer coefficient k (m s^{-1}) can be defined as the ratio of the total solute mass flux j_S into the channel and the difference between wall and bulk concentrations per unit volume ρC_w, ρC_b. It can be made dimensionless as a Sherwood number:

$$\mathrm{Sh} = \frac{j_S}{(C_w - C_b)} \cdot \frac{d_{eq}}{\rho D} \tag{2}$$

in which d_{eq} is the hydraulic diameter of the channel (4×area/wetted perimeter).

Also diffusive and convective Sherwood numbers can separately be defined as

$$\mathrm{Sh}_{diff} = \frac{j_{diff}}{(C_w - C_b)} \cdot \frac{d_{eq}}{\rho D} = -\frac{d_{eq}}{(C_w - C_b)} \left(\frac{\partial C}{\partial y} \right)_w \tag{3}$$

$$\mathrm{Sh}_{conv} = \frac{j_{conv}}{(C_w - C_b)} \cdot \frac{d_{eq}}{\rho D} = \frac{C_w}{(C_w - C_b)} \cdot \frac{v d_{eq}}{D} \tag{4}$$

in which the group vd_{eq}/D in Eq. (4) can be regarded as a transpiration Péclet number, Pe_{tr}. The total Sherwood number is then given by

$$\mathrm{Sh}=\mathrm{Sh}_{diff}+\mathrm{Sh}_{conv} \tag{5}$$

Figure 4 compares qualitative concentration profiles and mass fluxes for channels with transpiring and non-transpiring walls for a given C_b and a given solute mass flux j_S into the fluid.

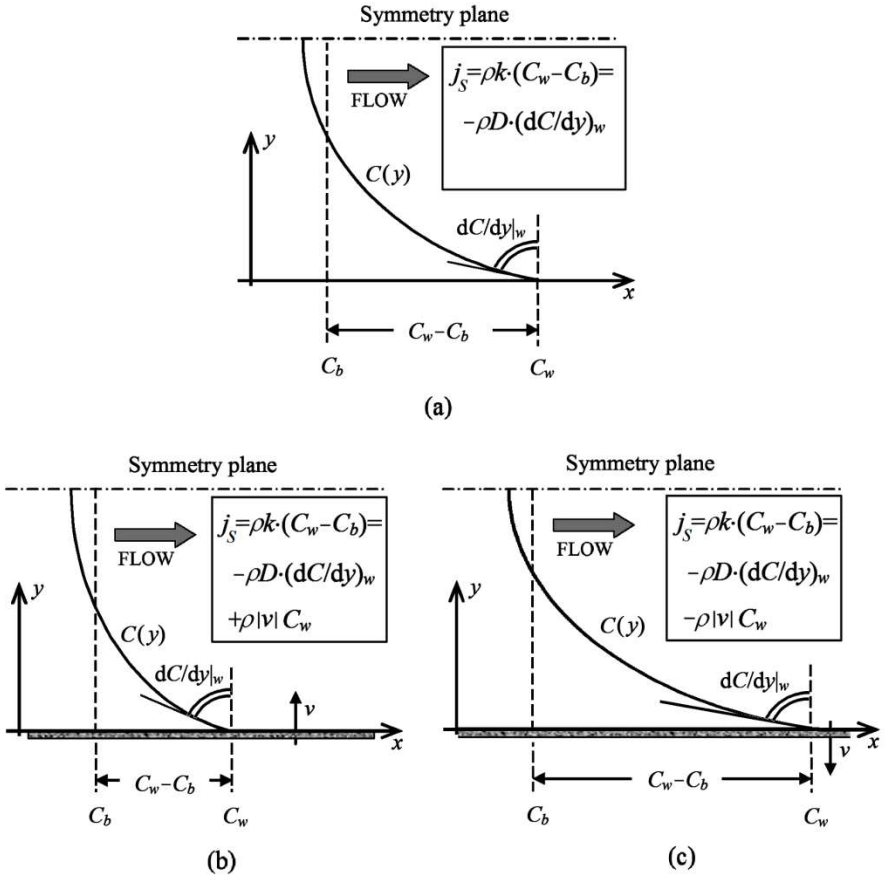

Figure 4. Concentration profiles and mass fluxes for transpiring and non-transpiring walls at the same bulk concentration C_b and mass flux j_S. (a) No transpiration. (b) Positive transpiration (blowing). (c) Negative transpiration (suction).

Graph (a) is for no transpiration; in this case, the mass flux at the wall is purely diffusive. Graph (b) is for a channel with positive transpiration (injection, or blowing, $v>0$). Here C_w, C_w-C_b and the diffusive mass flux $-\rho D(\partial C/\partial y)_w$ decrease with respect to the non-transpiring case (a), but this reduction is compensated by a positive (into the fluid) convective mass flux $\rho|v|C_w$, so that the overall mass transfer coefficient k increases. On the contrary, graph (c) is for a channel with negative transpiration (suction, $v<0$) of the same intensity as in case (b). Here C_w, C_w-C_b and the diffusive

mass flux $-\rho D(\partial C/\partial y)_w$ increase with respect to the non-transpiring case (a), but this increment is compensated by a negative (out of the fluid) convective mass flux $-\rho|v|C_w$, so that the overall mass transfer coefficient k decreases with respect to the no transpiration case.

2.2 Examples of mass transfer processes involving wall transpiration

As illustrated in Figure 5, electromembrane processes, and in particular reverse electrodialysis (RED) and electrodialysis (ED) [8, 9], exhibit the whole possible range of sign combinations for the fluxes of solute (salt) and solvent (water) into or from the channels.

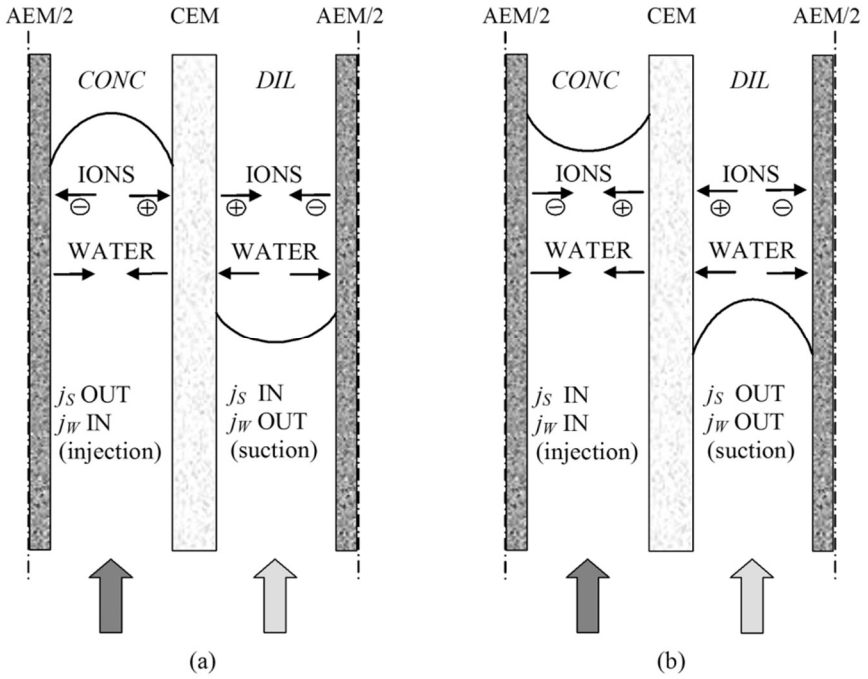

Figure 5. Concentrations and fluxes in cell pairs for reverse electrodialysis (a) or electrodialysis (b), exhibiting all possible sign combinations of solute (salt) and solvent (water) fluxes.

In particular, in reverse electrodialysis, Figure 5(a), electrical energy is harvested from the salinity gradient between two solutions. The figure shows a repetitive unit (cell pair) of a RED stack, including a concentrate channel (*CONC*), a diluate channel (*DIL*), an Anion Exchange Membrane (AEM) and a Cation Exchange Membrane (CEM). With ideal membranes, only anions and cations (e.g., Cl^- and Na^+) would flow from *CONC* to *DIL*. However, real membranes exhibit a non-null osmotic permeability, so that water flows from the dilute to the concentrate solution. Therefore, in the concentrate channels salt (in ionic form) flows out of the solution while water enters it (injection); on the contrary, in the diluate channels salt flows into the solution while water exits it (suction).

Conversely, in electrodialysis, Figure 5(b), electrical energy is used to create or enhance a salinity gradient between two solutions. The figure shows a cell pair, physically identical to a RED one. In the presence of osmotic fluxes, in the concentrate channels both salt and water flow into the solution, while, in the diluate channels, both salt and water flow out of the solution.

There are also processes in which, despite the net solute mass flux being nil, a mass transfer problem is involved in design and performance prediction [10]. Figure 6 shows the main mass transfer phenomena occurring in cross-flow filtration and reverse osmosis (RO). Here the wall is a selective membrane and the driving force is a trans-membrane pressure, pushing the continuous phase (solvent) out of the duct while the passage of the dispersed phase (solute) is prevented. The solute concentration builds up near the wall, causing a wall-to-fluid diffusive flux of solute $j_{diff} = -\rho D(\partial C/\partial y)$. At the same time, the (negative) y-component v of the solvent velocity causes a convective flux $j_{conv} = \rho v C$ directed from the fluid to the wall. At the wall (y=0), the two fluxes compensate each other (for a perfectly selective membrane), so that

$$j_S = -\rho D(\partial C/\partial y)_w + \rho v C_w = 0 \tag{6}$$

which is just a special case of Eq. (1).

The main problem is usually that of determining the trans-membrane pressure Δp to be applied to provide a given flux v of solvent (or *vice versa*). This would be trivial if v depended only on Δp, but is made more complex by the fact that it depends also on the near-wall concentration C_w (concentration polarization phenomenon). Eq. (6) can be regarded as a third type (Robin) wall boundary condition for the concentration C, allowing – once v is imposed – the solution of a solute transport equation and thus the assessment of C_w [11]. If the diffusive mass transfer coefficient k_{diff} (i.e., the diffusive Sherwood number Sh_{diff}) is known, the solution of the C-transport equation is not required since one has $-D(\partial C/\partial y)_w = k_{diff}(C_w - C_b)$, which, together with Eq. (6), gives $C_w = k_{diff} C_b /(k_{diff} + v)$.

Once v is imposed and the resulting near-wall solute concentration C_w is known, an independent equation linking the trans-membrane pressure with v and C_w is required. For example, in RO such equation can be derived from the Spiegler-Kedem model [11]:

$$v = -K\,[\Delta p - \sigma \Delta \pi(C_w)] \tag{7}$$

in which K is a permeability coefficient, σ is a rejection coefficient (close to 1) and Δp, $\Delta \pi$ are the static and osmotic trans-membrane pressure differences (internal−external), the latter being a function of C_w. Together, Eqs. (6) and (7) (in conjunction with either the solution of a transport

equation for C or the knowledge of Sh_{diff}) allow the prediction of the value of Δp necessary to obtain a prescribed water flux v, or *vice versa*.

In *filtration* problems (including microfiltration, ultrafiltration, nanofiltration) Eq. (7) is replaced by equivalent relations linking the trans-membrane Δp to the water flux and the near-wall concentration, for example by expressing the permeability coefficient K as a function of C_w.

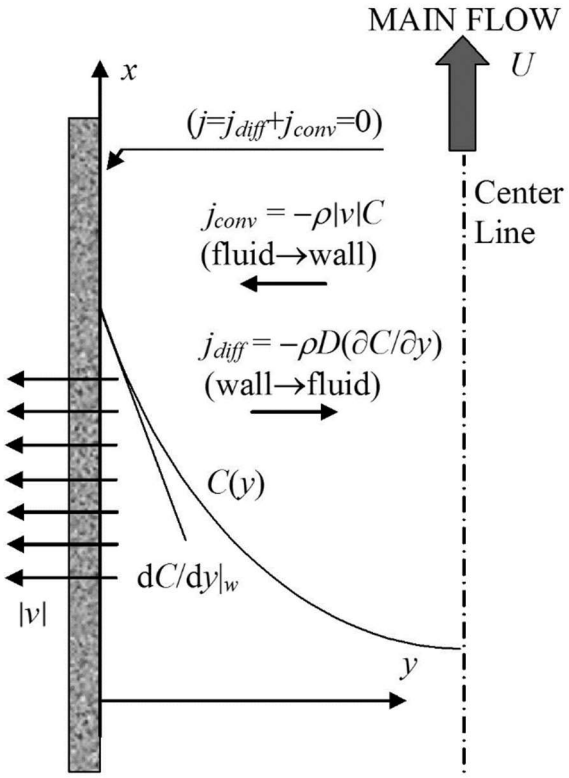

Figure 6. Mass transfer in cross-flow filtration and reverse osmosis, with zero net solute flux.

3. Simple model

3.1 Configuration studied and basic assumptions

The configuration considered in this study is laminar flow in a constant-cross section straight duct, as schematically illustrated in Figure 7. The duct has length l in the x-direction, cross sectional area A and wet perimeter P (hence, hydraulic diameter $d_{eq}=4A/P$). The working fluid (solution) enters with uniform velocity U_i and concentration (solute mass fraction) C_i. Both solute (with mass flux j_S) and solvent (with mass flux j_W) can cross the transpiring wall; j_S and j_W are positive for inflow, negative for outflow. Generic velocity and concentration profiles are shown.

Although the problem's treatment and the results are quite more general, this configuration can be regarded as representative of a flat rectangular channel belonging to a stack for electrodialysis,

reverse electrodialysis or similar membrane processes, as shown in Figure 5. When dimensioned quantities will be considered, the solvent will be assumed to be water and the solute an electrolyte such as NaOH with a Schmidt number of 500. The channel thickness H will be assumed to be 300 μm ($3\cdot10^{-4}$ m) and the length l to be 0.6 m, so that the hydraulic diameter d_{eq} (identifiable, in this case, with $2H$) will be $6\cdot10^{-4}$ m (l/d_{eq}=1000).

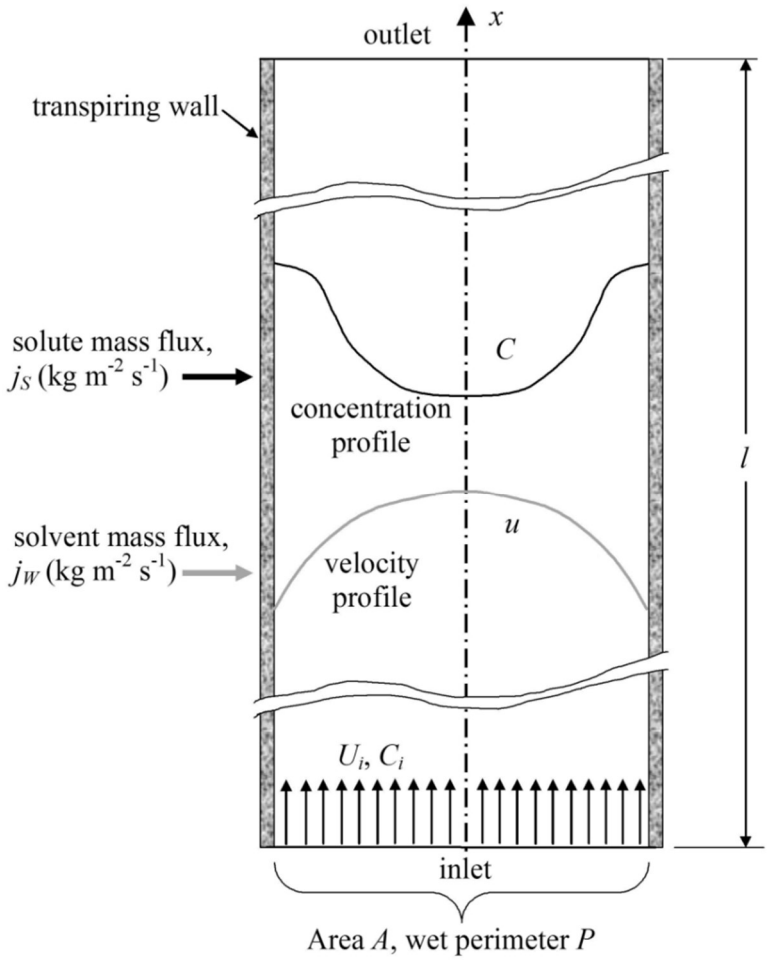

Figure 7. Sketch of the configuration studied (straight duct of length l, cross sectional area A and wet perimeter P with transpiring walls). Generic velocity and concentration profiles are shown. Both solute and solvent fluxes are positive if they enter the duct. U_i, C_i are uniform inlet velocity and concentration.

3.2 Axial velocity and concentration profiles

Mean velocity U and bulk concentration C_b along the channel can be obtained by elementary integral mass balances between the inlet at x=0 and the generic location x, provided j_S and j_W are known. In particular, for uniform j_S and j_W, the mass flow rates of solute (S) and solvent (W) are:

$$G_S(X) = \rho_i U_i C_i A\left(1 + \mathrm{Fl}^* X\right) \tag{8}$$

$$G_W(X) = \rho_i U_i A\left(1 - C_i + \mathrm{Tr}^* X\right) \tag{9}$$

in which $X=4x/d_{eq}$ is a dimensionless axial coordinate and Fl^*, Tr^* are two dimensionless numbers:

$$\mathrm{Fl}^* = \frac{j_S}{\rho_i U_i C_i} \qquad \text{(flux number)} \tag{10}$$

$$\mathrm{Tr}^* = \frac{j_W}{\rho_i U_i} \qquad \text{(transpiration number)} \tag{11}$$

Both Fl^* and Tr^* are defined with reference to the inlet conditions ρ_i, U_i, C_i; ρ_i is the solution density corresponding to the inlet concentration C_i, i.e. $\rho_i=\rho(C_i)$. The transpiration number Tr^* expresses the importance of the transpiration cross-flow with respect to the inlet axial flow, and is similar to the "blowing factor" used in the analysis of transpired boundary layers [1]. It is positive for blowing (injection), negative for suction. The flux number Fl^* expresses the importance of the solute mass flux crossing the walls with respect to the solute mass flux entering the channel from the inlet; also Fl^* is positive for mass flow into the channel, negative for mass flow out of it.

On the basis of Eqs. (8)-(9) and definitions (10)-(11), the bulk concentration at the generic location X can exactly be expressed as:

$$C_b(X) = \frac{G_S}{G_S + G_W} = C_i \frac{1 + \mathrm{Fl}^* X}{1 + \left(\mathrm{Tr}^* + C_i \mathrm{Fl}^*\right) X} \tag{12}$$

while the mean velocity of the solution can be obtained as

$$U(X) = \frac{G_S + G_W}{A\rho(X)} = \frac{U_i \rho_i + \left(j_W + j_S\right) X}{\rho(X)} \tag{13}$$

in which $\rho(X)= \rho(C_b(X))$. The dependence of the solution density upon the concentration is an empirical issue and is well documented for most common solutes (see for example reference [12]).

3.3 Limits

In an internal-flow configuration like that considered here, solvent and solute fluxes cannot be made to vary arbitrarily, but are subject to precise physical limitations. In particular, in the case of suction, j_W (<0) is limited by the requirement that the solvent mass flow rate G_W must remain positive at the outlet $x=l$. In terms of the dimensionless number Tr^*, taking Eq. (9) into account, the above limitation becomes

$$\mathrm{Tr}^* \geq -\frac{1 - C_i}{L} \qquad \text{("drying" limit)} \tag{14}$$

in which $L=4l/d_{eq}$ is the dimensionless channel length.

Similarly, in the case of solute flux out of the channel, j_S (<0) is limited by the condition that the solute mass flow rate must remain positive at the outlet $x=l$. In terms of the dimensionless number Fl^*, taking Eq. (8) into account, the above limitation becomes

$$\mathrm{Fl}^* \geq -\frac{1}{L} \qquad \text{(“desalting” limit)} \qquad (15)$$

For example, for $L=4000$ and $C_i \ll 1$, the common lower limit of Tr^* and Fl^* is $-2.5\cdot10^{-4}$.

For positive transpiration (injection) and/or solute flux there are, in principle, no such limits. In real applications, however, a further constraint arises by the requirement that the bulk concentration does not exceed anywhere some solubility limit ($C_b \leq C_{sat}$). The bulk concentration C_b provided by Eq. (12) is constant ($=C_i$) only for $\mathrm{Tr}^*=\mathrm{Fl}^*(1-C_i)$ (which includes the trivial case $\mathrm{Fl}^*=\mathrm{Tr}^*=0$), and varies monotonically with X otherwise. Therefore, it is sufficient to ensure that $C_b \leq C_{sat}$ for $X=L$, which yields

$$\mathrm{Fl}^* \leq \frac{C_{sat}}{C_i\left(1-C_{sat}\right)}\left[\frac{1}{L}\left(1-\frac{C_i}{C_{sat}}\right)+\mathrm{Tr}^*\right] \qquad \text{(“saturation” limit)} \qquad (16)$$

The constraints expressed by Eqs. (14)-(16) are schematically illustrated in Figure 8. Note that, for $C_{sat}<1$, the “no saturation” condition implies the “no drying” one, so that this becomes redundant. Only if no solubility limit exists, $C_{sat}=1$ and Fl^* in Eq. (1) diverges, meaning that the “saturation” limit coincides with the “drying” limit.

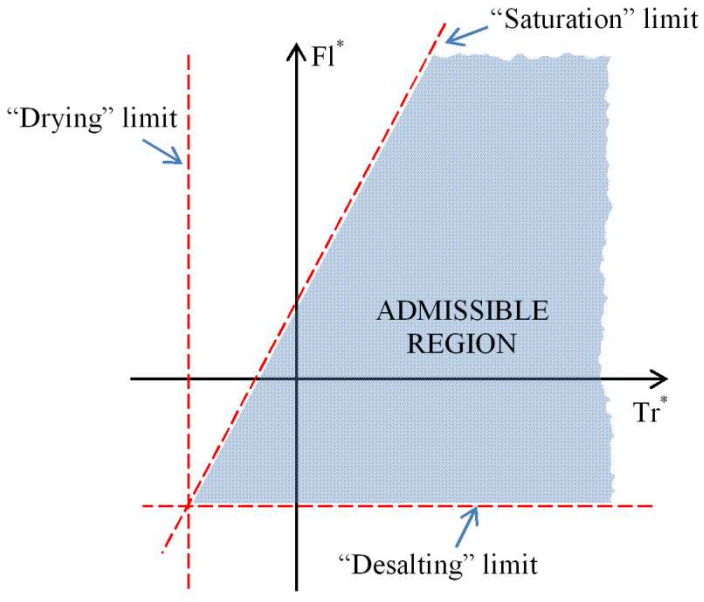

Figure 8. Constraints on the admissible values of Tr^* and Fl^* for given C_i and L.

Note also that the admissible region is unlimited on the right and that, for a given C_{sat}, the specific limiting values depend on C_i and L. Conversely, for given Tr^* and Fl^*, the limiting conditions can be regarded as constraints on the admissible values of C_i and L.

If the cross-stream concentration *profiles* were taken into account, the physical requirement that the concentration remains limited between 0 and C_{sat} everywhere across the channel would impose constraints more stringent than those expressed by Eqs. (14)-(16).

3.4 Simplifying assumption

In general, transpiration can be expected to distort the cross-stream profiles of both axial velocity u and concentration C with respect to the non-transpiring case, making an elementary analysis impossible and calling for a two- or three-dimensional computational approach.

A great simplification is obtained by assuming that concentration profiles across the channel are not excessively perturbed by transpiration, so that they remain self-similar at different transpiration intensities. Under this assumption, the diffusive Sherwood number Sh_{diff}, Eq. (3), coincides with that obtained under no-transpiration conditions, Sh_0, which depends on the duct's geometry and on the boundary conditions. In the fully developed region, it is exactly known from analytical solutions for parallel flow in simple ducts such as circular pipes or plane channels.

For physical reasons, the above approximation is the more accurate the smaller the transpiration intensity. In section 4, quantitative limits to the validity of the approximation will be derived from CFD numerical simulations, and it will be shown that it depends also on the Schmidt number. Here, we will draw consequences from the approximation assuming only that the transpiration intensity is sufficiently small for it to hold.

Under the assumption $\mathrm{Sh}_{diff}=\mathrm{Sh}_0$, from Eqs. (2-5) one has:

$$j_S = j_{diff} + j_{conv} = \mathrm{Sh}_0 (C_w - C_b)\frac{\rho D}{d_{eq}} + j_W C_w \tag{17}$$

For any given C_b, if the transpiration flux j_W and the wall concentration C_w are known, then Eq. (17) directly provides the total solvent mass flow rate j_S. Conversely, if both the solute and the solvent mass flow rates j_S, j_W are known, then the wall concentration can be obtained by solving Eq. (17) for C_w:

$$C_w = \frac{j_S + \mathrm{Sh}_0 C_b \rho D / d_{eq}}{j_W + \mathrm{Sh}_0 \rho D / d_{eq}} \tag{18}$$

Eqs. (17) and (18) completely solve the problem of determining j_S for a given C_w or *vice versa*, once the local bulk concentration C_b is known.

3.5 Dimensionless formulation

The above results can be cast into a more elegant and physically meaningful form by expressing the total Sherwood number Sh as a function of dimensionless parameters.

To this purpose, let us consider a generic cross section along the channel. Besides the flux and transpiration numbers defined by Eqs. (10) and (11), which are based on *inlet* conditions, it is convenient to define *local* dimensionless numbers

$$\mathrm{Pe} = \frac{U d_{eq}}{D} \qquad \text{(local Péclet number)} \tag{19}$$

$$\mathrm{Fl} = \frac{j_S}{\rho U C_b} \qquad \text{(local flux number)} \tag{20}$$

$$\mathrm{Tr} = \frac{j_W}{\rho U} \qquad \text{(local transpiration number)} \tag{21}$$

in which ρ and D are the solution density and the solute diffusivity corresponding to the local bulk concentration C_b.

With some algebraic manipulations and taking account of the definitions in Eqs. (2) and (19)-(21), Eq. (17) can be written as

$$\frac{\mathrm{Sh}}{\mathrm{Sh}_0} = \frac{1 + \mathrm{Tr} \cdot \mathrm{Pe} / \mathrm{Sh}_0}{1 - \mathrm{Tr} / \mathrm{Fl}} \tag{22}$$

This shows that, under the assumption of self-similar concentration profiles, $\mathrm{Sh}/\mathrm{Sh}_0$ is a function of the dimensionless numbers Fl, Tr and Pe. For a given value of Pe, an isoline map of $\mathrm{Sh}/\mathrm{Sh}_0$ can be plotted in the (Tr, Fl) plane as shown in Figure 9 for $\mathrm{Pe}=10^4$.

The insets surrounding Figure 9 schematically show the direction of solvent and solute fluxes and the concentration profile associated to each value, or range of values, of the polar coordinate θ defined by $\mathrm{Fl}/\mathrm{Tr}=\tan(\theta)$. Left and lower boundaries (dash-dot lines) roughly correspond to the "drying" and "desalting" limits expressed by Eqs. (14)-(15); the correspondence is not exact because these latter limits are expressed in terms of Tr^* and Fl^* (based on inlet conditions), and not in terms of the present (local) numbers Tr, Fl. In the top direction the map would be limited by the "saturation" condition expressed by Eq. (16), which was not reported here for simplicity.

The map can be divided into several regions differing in the sign and relative importance of Tr and Fl and in the values correspondingly attained by the normalized Sherwood number $\mathrm{Sh}/\mathrm{Sh}_0$.

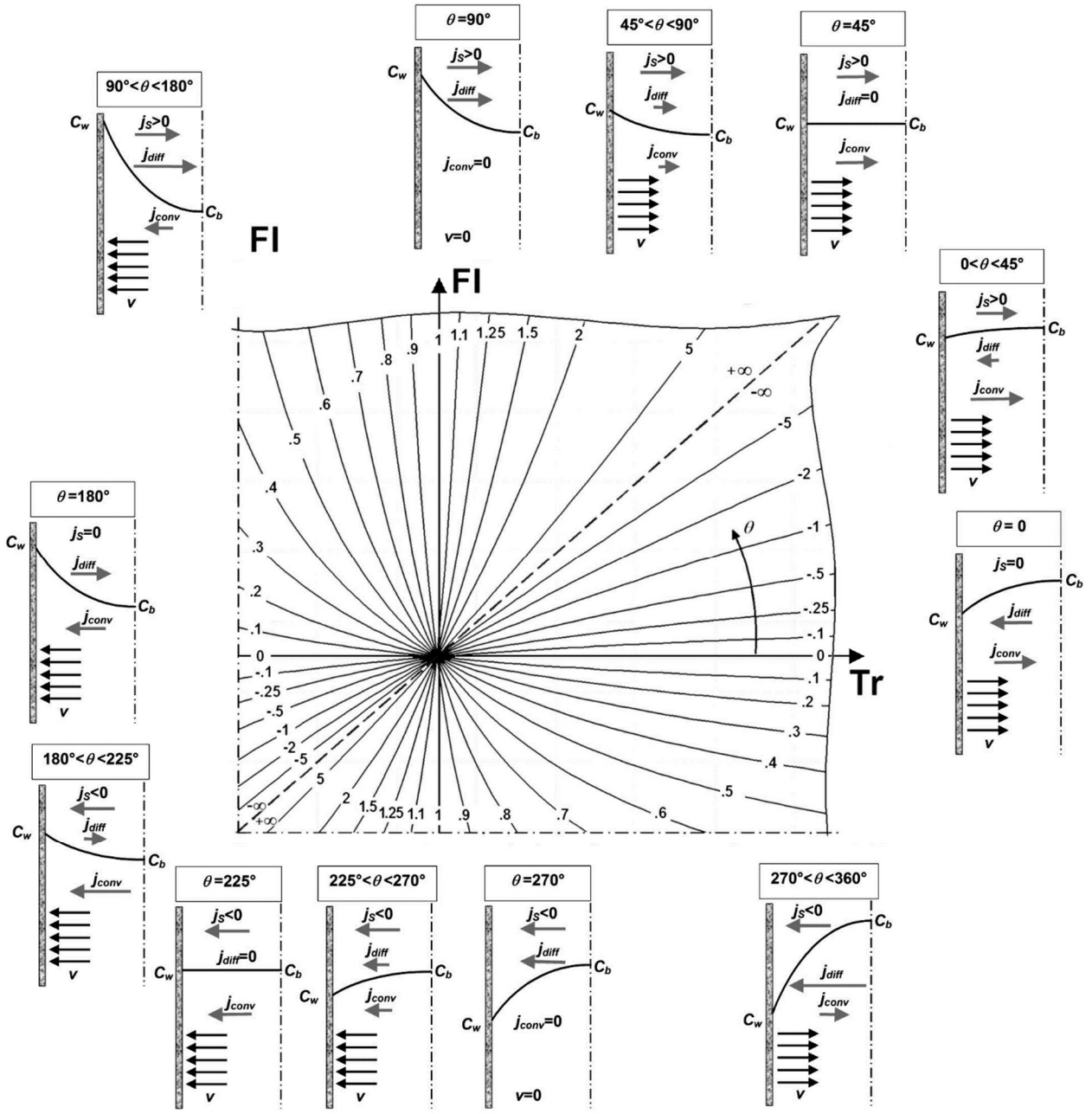

Figure 9. Lines Sh/Sh_0=constant in the (Tr, Fl) plane for $Pe=10^4$.

- For θ=0, i.e. along the Tr>0 half of the horizontal axis Fl=0, the net solute flux is nil but a positive solvent transpiration flux exists (except at the origin), creating a concentration profile and a (negative) concentration drop $\Delta C=C_w-C_b$. Therefore, one has Sh=0. The origin itself is obviously a singular case in which neither solvent nor solute fluxes exist and Sh is undefined.
- For $0<\theta<45°$, both the solute and the solvent fluxes are positive (Tr>0, Fl>0) but the convective solute flux is larger than the diffusive one (Tr>Fl) so that the wall concentration is still lower

than the bulk concentration, yielding $\Delta C<0$ and thus Sh<0.

- For $\theta=45°$, i.e. along the bisecting line Fl=Tr (with Fl>0, Tr>0), the solute influx is purely convective, so that $\Delta C=0$ and Sh diverges to $-\infty$ on the side $\theta<45°$ and to $+\infty$ on the opposite side $\theta>45°$.
- For $45°<\theta<90°$, both the solute and the solvent fluxes are still positive (Tr>0, Fl>0), but the convective solute flux is less than the diffusive one (Tr<Fl); $\Delta C=C_w-C_b$ is now positive but less than it would be for the same j_S in the absence of transpiration, so that Sh exceeds Sh_0. This is the range in which blowing promotes mass or heat transfer from the wall to the fluid.
- For $\theta=90°$, i.e. along the vertical axis (Tr=0, Fl>0), the classic condition of mass transfer from the wall to the fluid without transpiration is recovered, and Sh attains its reference value Sh_0.
- For $90°<\theta<180°$, one has Tr<0, Fl>0. The convective solute flux is negative but less, in absolute value, than the diffusive solute flux; for a given total solute flux, the diffusive component and $\Delta C=C_w-C_b$ (>0) are larger than for $\theta=90°$, so that Sh becomes less than Sh_0. This is the range in which suction inhibits mass or heat transfer from the wall to the fluid.
- The case $\theta=180°$ (left part of the horizontal axis Fl=0) is similar to the case $\theta=0$: the solute flux is nil but a negative solvent transpiration flux exists, creating a concentration profile and a (positive) concentration drop C_w-C_b. Therefore, Sh=0. This case is, basically, that discussed in Section 2.2 for reverse osmosis or filtration (Figure 6).
- For $180°<\theta<225°$, both the solute and the solvent fluxes are negative (Tr<0, Fl<0) but the convective solute flux dominates over the diffusive one ($|\mathrm{Tr}|>|\mathrm{Fl}|$), so that the wall concentration becomes higher than the bulk concentration and Sh<0.
- For $\theta=225°$, i.e. along the bisecting line Fl=Tr (with Fl<0, Tr<0), the solute flux is purely convective, so that $C_w-C_b=0$ and Sh diverges to $-\infty$ on the side $\theta<225°$ and to $+\infty$ on the opposite side $\theta>225°$.
- For $225°<\theta<270°$, both the solute and the solvent fluxes are still negative (Tr>0, Fl>0), but the solvent inflow is relatively small ($|\mathrm{Tr}|<|\mathrm{Fl}|$); the result is a reduction of $|C_w-C_b|$ (with C_w-C_b negative) and an increment of Sh with respect to the non-transpiring case ($Sh>Sh_0$). This is the range in which suction promotes mass or heat transfer from the fluid to the wall.
- For $\theta=270°$, i.e. along the vertical axis (Tr=0, Fl<0), the classic condition of mass transfer (from fluid to wall) without transpiration is recovered, as in the case $\theta=90°$, and $Sh = Sh_0$.
- Finally, for $270°<\theta<360°$, one has Tr>0, Fl<0. The convective solute flux at the wall is positive but less, in absolute value, than the total (negative) solute flux; for a given total solute flux, the

diffusive component and $|C_w\text{-}C_b|$ increase (C_w-C_b is negative) with respect to the no-transpiration case, so that Sh becomes less than Sh_0. This is the range in which blowing inhibits mass transfer from fluid to wall (mass transfer analogue of transpiration cooling).

Note that the singularities at θ=45° and 225° correspond to the condition Fl=Tr. Under this condition, the combined effect of solvent and solute inflow or outflow is equivalent to the inflow or outflow of solution having a concentration equal to the bulk concentration in the channel, a condition for which $j_S \neq 0$ but $C_w - C_b = 0$, hence $Sh = \pm\infty$.

Figure 9 suggests that not only the qualitative behaviour of the solution, but also the ratio Sh/Sh_0 is mainly a function of the polar coordinate θ. In fact, an analysis of Eq. (22) shows that, for small values of the group $Tr \cdot Pe/Sh_0$, one has $Sh/Sh_0 \approx (1\text{-}Tr/Fl)^{-1}$, i.e. Sh/Sh_0 is a function of the single dimensionless number $Fl/Tr = \tan(\theta)$ (ratio of flow and transpiration numbers). For larger values of $Tr \cdot Pe/Sh_0$, Sh/Sh_0 in Eq. (22) becomes a function of Tr and Fl separately, and not only of their ratio. This behaviour corresponds to the departure of the iso-lines in Figure 9 from straight lines crossing the origin, a departure which is particularly visible in the second and fourth quadrants where Fl and Tr have opposite signs.

Figure 10 reports the normalized Sherwood number along a circle of radius 10^{-4} in the (Tr, Fl) plane for Pe ranging from $3 \cdot 10^3$ to 10^5.

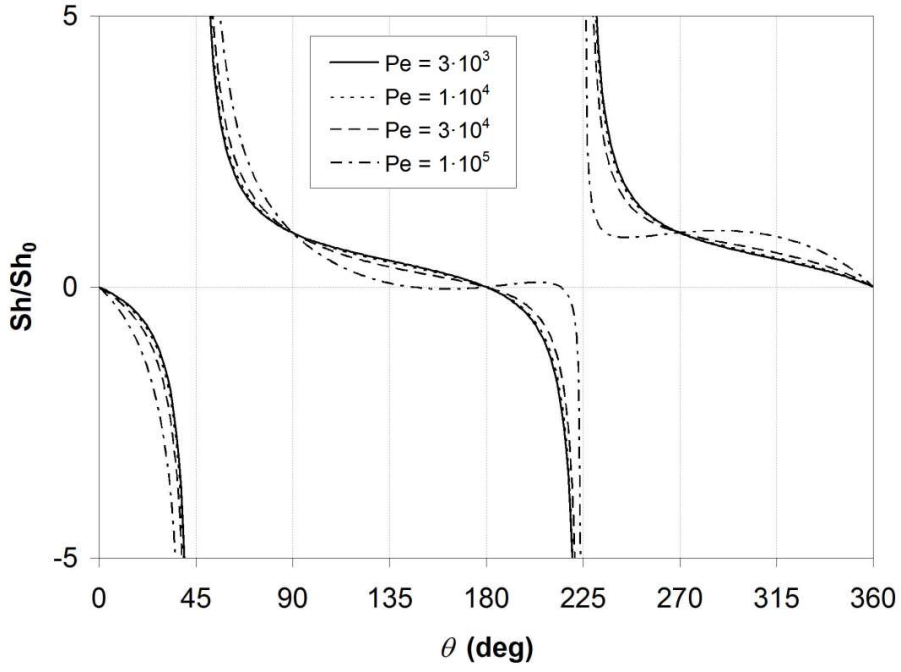

Figure 10. Normalized Sherwood number as a function of the azimuthal angle θ (see Figure 11) for $(Tr^2+Fl^2)=10^{-8}$ and different values of the Péclet number, ranging from $3 \cdot 10^3$ to 10^5.

It can be observed that, for Pe up to ~$3\cdot10^4$, Sh/Sh_0 does not appreciably depend on the Péclet number. Also, for such small values of Pe, the function $Sh(\theta)$ is periodic with period 180°, so that the simultaneous reversal of Tr and Fl leaves Sh unchanged. Only at higher values of Pe (e.g. 10^5) Sh becomes a function of Pe and the 180°-periodicity is lost.

3.6 Axial profiles and entrance effects

The simple model has the potential to predict not only local quantities, but also the axial (streamwise) profile of the Sherwood number. In fact, if the inlet concentration and velocity C_i, U_i are known, Eqs. (12) and (13) can be used to compute bulk concentration and mean velocity C_b, U at any location x. Local Péclet, transpiration and flux numbers can be recomputed for each x by Eqs. (19)-(21), and then Eq. (22) provides the local Sherwood number Sh.

Entrance effects can be taken into account by the Graetz theory [14]. For laminar flow in ducts with no transpiration, this predicts that the local Sherwood number decreases towards its fully developed value Sh_∞ as a function of the dimensionless Graetz number, $Gz=Pe\cdot d_{eq}/x$ (or, in the present notation, $Gz=4Pe/X$). For plane channels one has $Sh/Sh_\infty<1.05$ for $Gz<50$ [8]. In the present configuration, due to the high value of Sc (500) and despite the low values of Re (e.g. 8), Pe is relatively high (e.g. 4000), so that the condition Gz=50 is attained for $x/d_{eq}=80$. For H=300 μm (d_{eq}=600 μm) and l=0.6 m, this value corresponds to a distance of 0.08 l from inlet, which is a significant fraction of the channel length. An approximate formula, suitable for plane channels and rectangular channels of large aspect ratio [8], is:

$$\frac{\mathrm{Sh}}{\mathrm{Sh}_\infty} = C_G \left[\mathrm{Gz} + \left(\frac{1}{C_G} \right)^3 \right]^{1/3} \tag{23}$$

with the constant C_G equal to 0.18. Of course, Eq. (23) is not necessarily accurate for channels with transpiring walls; an evaluation of the accuracy of this correlation also in the presence of transpiration will be given on the basis of CFD results in Section 4.

3.7 An alternative formulation of the simple model

Eq. (22) can be simplified by observing that, in the light of the definitions given in Eqs. (19)-(21), the product $Tr\cdot Pe$ reduces to the transpiration Péclet number, $Pe_{tr} = vd_{eq}/D = j_W d_{eq}/(\rho D)$, while the ratio Fl/Tr reduces to $(j_S)/(C_b j_W)$. In this last expression, j_S/j_W can be interpreted as the equivalent concentration C_{eq} that the transpiring flow alone should possess in order to provide the actual solute

inflow or outflow j_S. Therefore, the ratio Fl/Tr can be interpreted as the ratio C_{eq}/C_b of equivalent to bulk concentration, and can be used as a new dimensionless number Cr (concentration ratio). Note that, when j_S and j_W have opposite signs, C_{eq} is negative and thus is not physically realizable.

Using the above definitions, Eq. (22) can be re-written as

$$\frac{\mathrm{Sh}}{\mathrm{Sh}_0} = \frac{1 + \mathrm{Pe}_{tr} / \mathrm{Sh}_0}{1 - 1/\mathrm{Cr}} \tag{24}$$

which expresses the ratio $\mathrm{Sh}/\mathrm{Sh}_0$ (normalized Sherwood number) as a function of two dimensionless numbers only, Pe_{tr} (transpiration Péclet number) and Cr (concentration ratio).

Figure 11 reports lines $\mathrm{Sh}/\mathrm{Sh}_0$=constant in the ($\mathrm{Pe}_{tr}$, Cr) plane. Pe_{tr} is normalized by Sh_0.

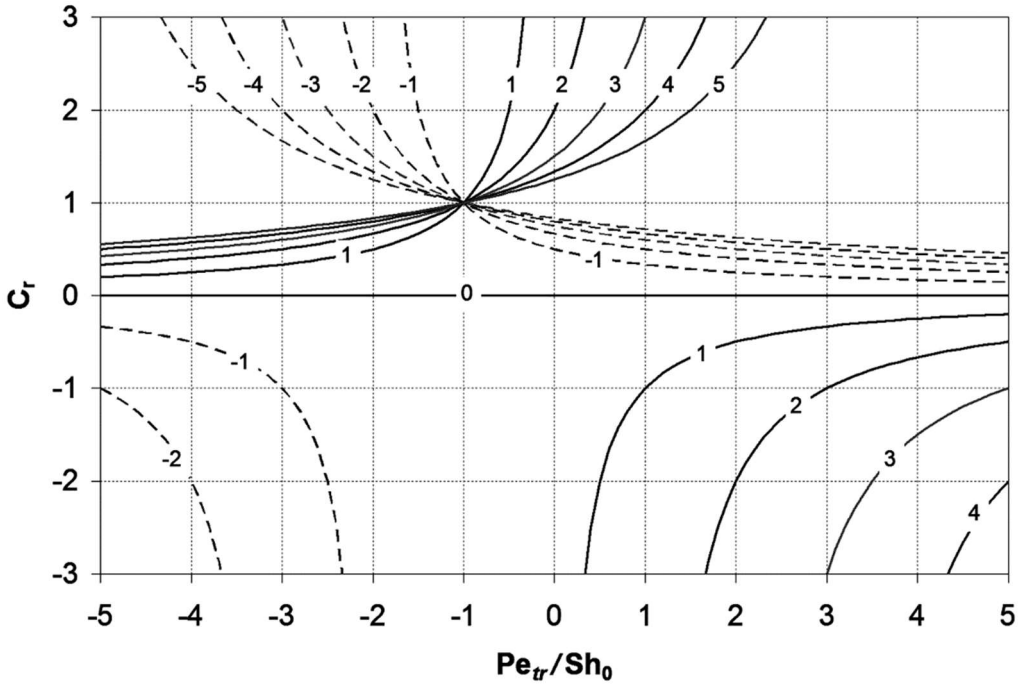

Figure 11. Lines $\mathrm{Sh}/\mathrm{Sh}_0$=constant in the ($\mathrm{Pe}_{tr}$, Cr) plane.

The line Cr=1 in Figure 11 corresponds to the asymptote Fl=Tr in Figure 9, where the denominator of both Eqs. (22) and (24) vanish. On this line the Sherwood number diverges everywhere except at the singular point $\mathrm{Pe}_{tr} = -\mathrm{Sh}_0$, for which also the numerator vanishes in Eqs. (22) and (24). Thus, the point ($\mathrm{Pe}_{tr}/\mathrm{Sh}_0 = -1$, Cr = 1) in Figure 11 corresponds to the origin in Figure 9, where Sh is undefined.

On the whole, despite involving only two dimensionless numbers instead of three, the representation of Figure 11, based on Eq. (24), is probably less physically meaningful and easy to interpret than the representation of Figure 9, based on Eq. (22).

4 CFD approach and comparison with the simplified model

4.1 Governing equations and boundary conditions

As far as C can be regarded as the concentration of a *massless passive scalar*, fluid flow and solute transport in the channel are governed by the following continuity, momentum (Navier-Stokes) and scalar transport equations, written for steady-state conditions and in tensor notation:

$$\frac{\partial \rho u_j}{\partial x_j} = 0 \tag{25}$$

$$\frac{\partial \rho u_i u_j}{\partial x_j} = -\frac{\partial p}{\partial x_i} + \frac{\partial}{\partial x_j}\mu\left(\frac{\partial u_i}{\partial x_j} + \frac{\partial u_j}{\partial x_i}\right) \tag{26}$$

$$\frac{\partial \rho u_j C}{\partial x_j} = \frac{\partial}{\partial x_j}\rho D \frac{\partial C}{\partial x_j} \tag{27}$$

Dirichlet, Neumann or mixed (Robin) conditions for C can be applied at the wall to simulate solute transfer. Transpiration can be described by means of a boundary mass source, either positive for injection or negative for suction, located at the wall. By this approach, the contribution of the solute to mass balance is neglected, which may become an unacceptable approximation if the solute mass flux, integrated over the walls, is a significant fraction of the total mass flow rate.

An alternative of more general validity is to treat the solution as a *variable composition mixture*, made up of two components: solute, with mass fraction C, and solvent, with mass fraction 1-C. The two components share a common velocity field **u**, so that the momentum equations (26) remain valid. The continuity equation (25) is replaced by separate continuity equations for the two components. Solute transport is still governed by Eq. (27), including diffusion terms. The flux of both components through the wall is described by suitable boundary mass sources expressing the mass flow rate of that component entering or leaving the fluid. This treatment allows the contribution of the solute to mass balance to be taken into account.

Both treatments were implemented into the finite volume CFD code Ansys-CFX®. As expected, they provided similar results for small inlet-outlet solute mass flow rate variations, but differed significantly otherwise; the variable composition mixture approach was preferred for its greater generality. Note that neither model distinguishes a “true” solution (i.e., a dispersion at molecular level, as may occur with salt water) from a heterogeneous, two-phase, dispersion (as may occur with suspended particles), provided the dispersion scale is sufficiently small for inter-phase slip to vanish and a single flow field to apply to both components. Therefore, for example, filtration problems at various scales can be treated by the same model as electrodialysis or reverse osmosis.

In either approach, the solution's physical properties (density ρ, viscosity μ) and the solute's diffusivity D – or, equivalently, the Schmidt number $(\mu/\rho)/D$ – should be expressed as functions of the concentration C, especially in the presence of strong spatial variations of this quantity. However, as mentioned above, in the present study we assumed constant values of the properties (ρ=1000 kg m^{-3}, μ=0.9·10^{-3} Pa·s, Sc=500), so as to avoid unnecessary complications in interpreting the results.

One half of a plane channel of indefinite width was simulated. Only two dimensions, streamwise (x) and cross-stream (y) were considered, and symmetry was imposed at the centreline. Dirichlet conditions $u=U_i$, $C=C_i$ were imposed at the inlet for axial velocity and concentration. At the outlet, a uniform pressure p_0 was imposed for the flow field and fully developed Neumann conditions ($\partial/\partial x$=0) for the concentration field C. As discussed above, at the transpiring wall solute and solvent fluxes were represented as boundary mass sources for the two components.

4.2 Validation of the self-similarity assumption

For the case of a plane channel of thickness H with Re=8 and Sc=500 (Pe=4000), Figure 12 shows cross-stream C profiles, normalized as $(C-C_b)/(C_w-C_b)$, computed by the CFD approach for Fl/Tr=2 and for the local transpiration number Tr increasing from 0 to 10^{-2}. For symmetry reasons, only one half of the channel ($0\leq y/H\leq 0.5$) is shown. It can be observed that up to Tr≈10^{-3} concentration profiles remain basically self-similar, while at higher values of Tr they develop an inflection point and become flat in the proximity of the wall, in correspondence with the decreasing relative importance of the diffusive mass flux.

A more complete CFD study, including different values of Sc and negative values of Tr, shows that the assumption of self-similar concentration profiles holds provided Sc·|Tr|«1. For example, for Sc=1 a significant departure from self-similarity would occur only at unlikely transpiration velocities of the same order as the inlet velocity. Similarly, normalized velocity profiles remain very close to the Poiseuille profile provided |Tr|«1.

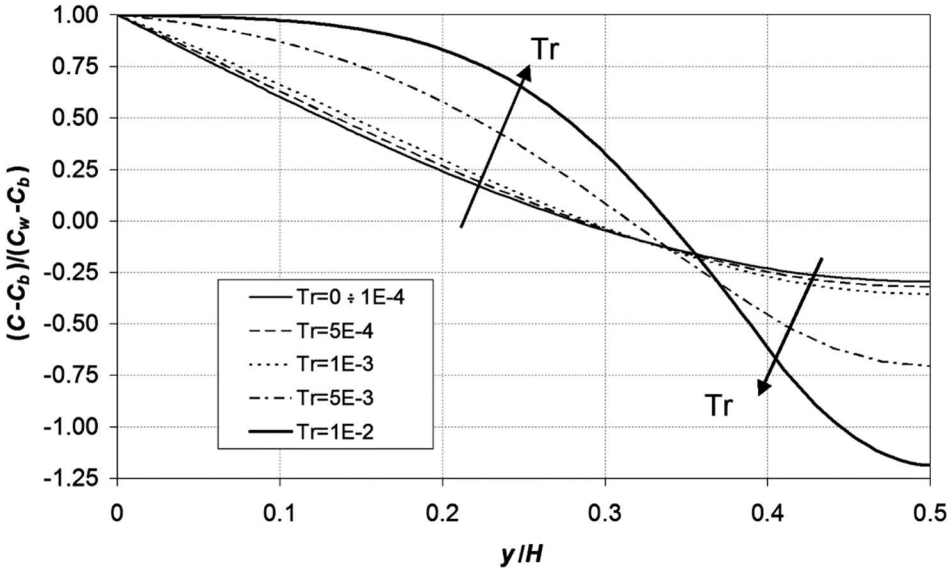

Figure 12. Cross stream profiles of concentration, normalized as $(C\text{-}C_b)/(C_w\text{-}C_b)$, computed by CFD for Sc=500, Re=8, Fl/Tr=2 and increasing values of the transpiration number Tr in the range 0 to 10^{-2}.

As long as normalized concentration profiles remain close to that holding in the absence of transpiration, also the diffusive Sherwood number Sh_{diff} defined by Eq. (3) remains close to the theoretical no-transpiration value Sh_0 (e.g. ~8.24 for plane channels with uniform imposed wall mass flux [13]). Figure 13 shows Sh_{diff} as a function of the transpiration number, computed by 2-D CFD under the same conditions as Figure 12 (Re=8, Sc=500, Fl/Tr=2).

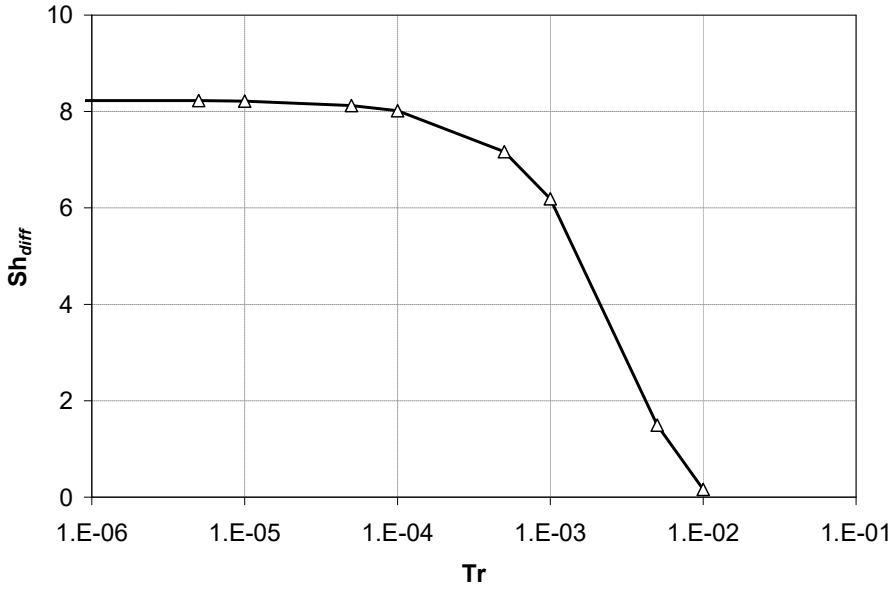

Figure 13. Diffusive Sherwood number Sh_{diff} as a function of the transpiration number Tr, computed by CFD for Sc=500, Re=8, Fl/Tr=2.

It can be observed that the diffusive Sherwood number remains approximately constant up to $Tr \approx 10^{-4}$, while, for Tr higher than $\sim 10^{-3}$, it falls rapidly and becomes negligible for $Tr = 10^{-2}$.

4.3 CFD Results and comparison with the simple model

A comparison of CFD results and approximate predictions provided by Eq. (22) (obtained under the assumption of self-similar concentration profiles, i.e. diffusion Sherwood number unaffected by transpiration) is shown in Figure 14. Here, for two values of the flux number, namely $Fl = -1.5 \cdot 10^{-4}$ (solute out of the channel) and $Fl = 1.5 \cdot 10^{-4}$ (solute into the channel), the normalized Sherwood number Sh/Sh_0 is reported as a function of the transpiration number Tr in the range from $-2 \cdot 10^{-4}$ to $2 \cdot 10^{-4}$. Figure 14 shows that the predictions of the approximate model agree well with CFD results in the range considered, which for Sc=500 complies with the above mentioned criterion $Sc \cdot |Tr| \ll 1$. Predictions (either by the approximate model or by CFD) should be taken with some caution in the proximity of the singular lines Tr=Fl.

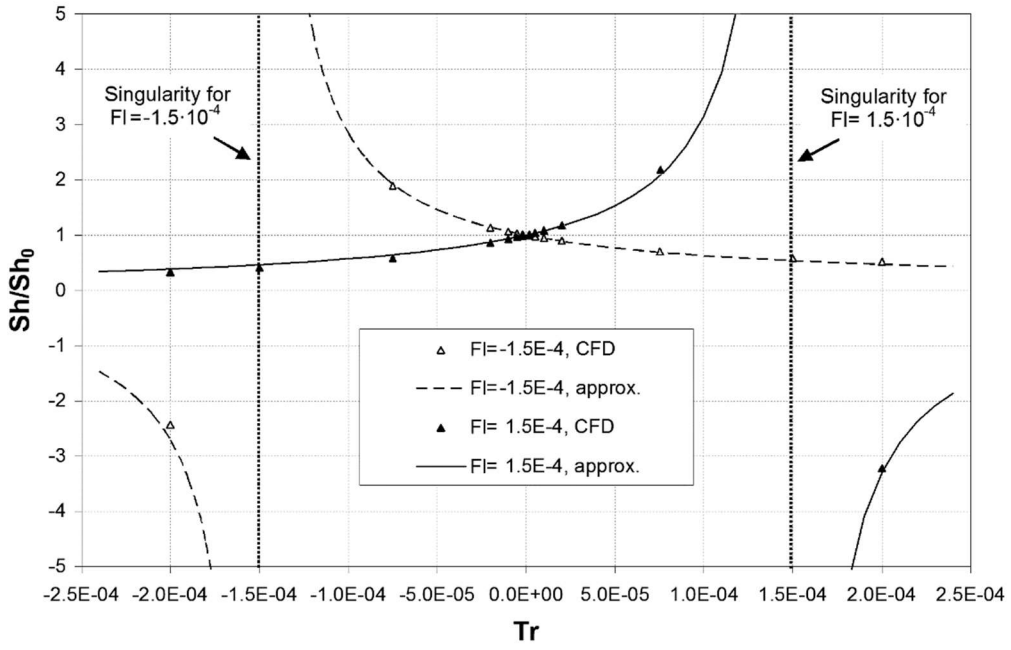

Figure 14. Normalized Sherwood number as a function of the transpiration number for flux numbers $Fl = \pm 1.5 \cdot 10^{-4}$. Approximate predictions provided by Eq. (22) are compared with CFD results. Hollow symbols and broken line: $Fl = -1.5 \cdot 10^{-4}$; solid symbols and solid line: $Fl = 1.5 \cdot 10^{-4}$.

As a comparison of space-dependent results, Figure 15 reports axial profiles of the Sherwood number along the channel walls for the same two values of the flux number Fl^* as in Figure 14, namely $-1.5 \cdot 10^{-4}$ (a) or $+1.5 \cdot 10^{-4}$ (b), $Pe^*=4000$, and transpiration numbers Tr^* increasing from

$-2\cdot10^{-4}$ to $2\cdot10^{-4}$. The abscissa is the normalized axial coordinate x/L. Results from the simplified model (solid lines) are compared with CFD predictions (broken lines), in which no simplifying assumption is made on the cross-stream concentration profiles and the diffusive Sherwood number. A fair agreement between the predictions of the simple model and CFD results can be observed; the largest discrepancies occur for large transpiration numbers and solvent/solute fluxes having the same direction. Entrance effects are satisfactorily captured, which encourages the use of Eq. (23) also in the presence of transpiration.

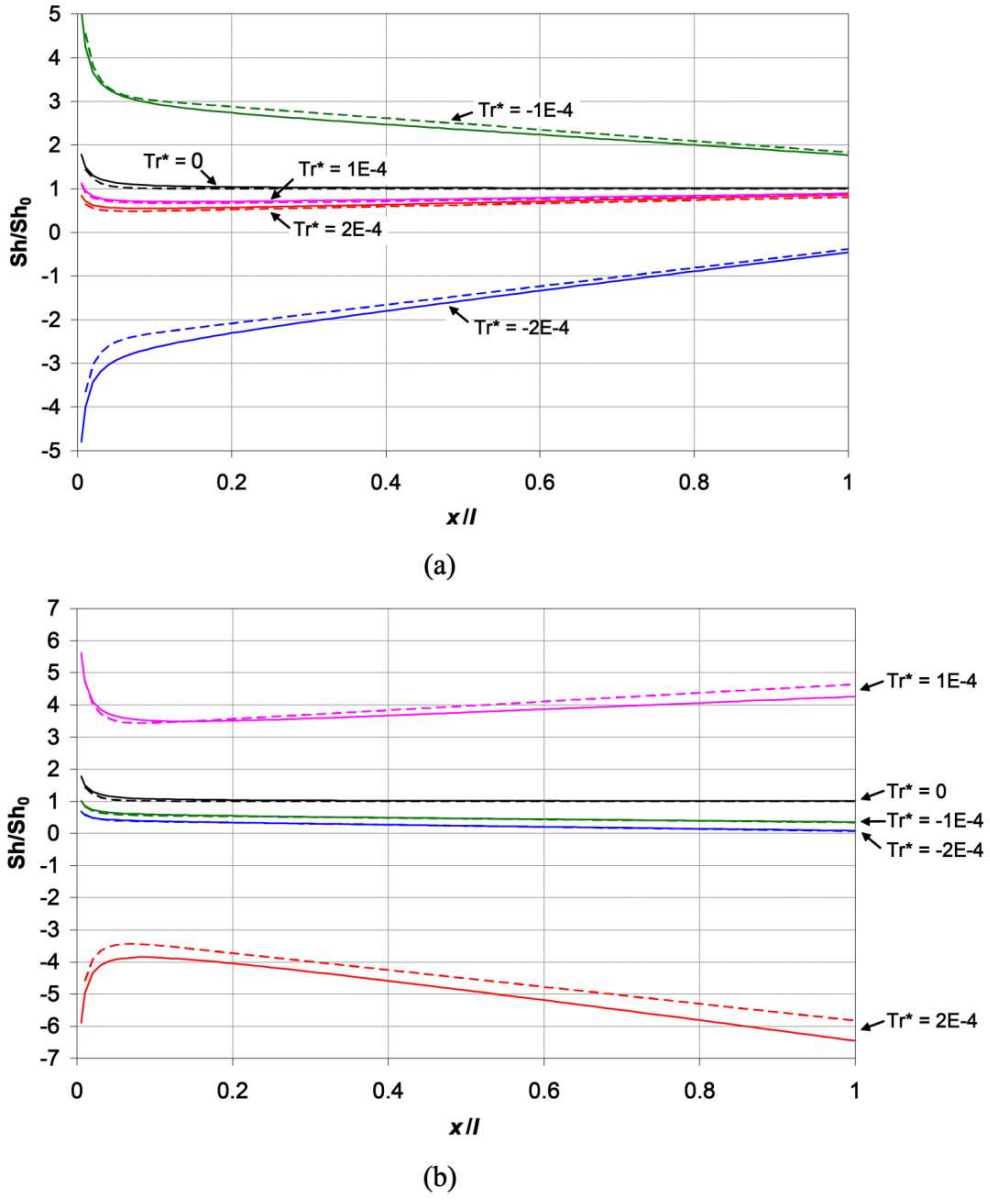

Figure 15. Axial profiles of the normalized Sherwood number along the channel walls for Pe^*=4000, flux number $Fl^* = -1.5\cdot10^{-4}$ (a) or $1.5\cdot10^{-4}$ (b), and transpiration numbers Tr^* ranging from $-2\cdot10^{-4}$ to $2\cdot10^{-4}$. Solid lines: present simple model; broken lines: CFD results.

The behaviour of Sh for each combination of Fl and Tr can be interpreted in the light of the map in Figure 9. A noteworthy feature of the results in Figure 15 is that, in the presence of transpiration, the Sherwood number does not tend to a constant value for large x, but continues to vary (almost linearly) along the channel. More precisely, as x increases, the Sherwood number profiles obtained for different Tr^* tend to converge to Sh_0 when the flux number Fl^* is negative (solute flux out of channel), whereas they diverge when Fl^* is positive (solute into channel).

5. Conclusions

Mass transfer between a fluid stream and a wall in the presence of cross-stream flow (wall transpiration) was analysed. A suitable notation was introduced, based on separately considering the fluxes of two components, a "solvent" and a "solute", through the wall. All possible configurations were classified according to the combined signs of the two fluxes, and special or singular conditions (including simple mass transfer with no transpiration) were identified. Examples from engineering, notably from membrane-based processes, were given for several of the more complex flux combinations; they include, among others, direct and reverse electrodialysis, reverse osmosis and filtration. The analogy with heat transfer processes involving transpiration (e.g. transpiration cooling) was also briefly discussed.

In the bulk of the paper, the attention was focussed on a specific configuration, namely, parallel flow in a straight duct of constant cross section with simultaneous solute flux and solvent transpiration at the walls. Besides the common dimensionless parameters occurring in no-transpiration problems, such as the Reynolds, Schmidt, Péclet and Sherwood numbers Re, Sc, Pe, Sh, new dimensionless numbers appropriate to transpiration problems were introduced. These include a transpiration number (Tr) and a flux number (Fl), respectively expressing the importance of the transpiration solvent flux and of the total solute flux through the walls with respect to the inlet flow rate and advection solute flux. Limiting values of these numbers, associated to what can be called the "drying", "desalting" and "saturation" conditions, were identified as functions of channel slenderness and inlet conditions.

The subsequent analysis was conducted for a high Schmidt number (500) and proceeded along two parallel directions.

On one side, the problem was analysed by computational fluid dynamics using a finite volume method. Solute transport was modelled by two different approaches: the former treated the solute as a passive and massless scalar, while the latter treated the solution as a variable composition mixture with separate continuity equations for solvent and solute. The two treatments converged for low concentrations, but only the latter properly accounted for the contribution of the solute to the

solution mass balance (important at high concentrations), and thus was preferred in the generality of the cases.

On the other side, a simplifying assumption was adopted, namely, that the transpiration flow does not significantly affect normalized concentration profiles and thus diffusive Sherwood numbers. By comparison with CFD simulations, this assumption was found to hold to a fair degree as far as the product of the Schmidt number and the transpiration number, $Sc \cdot Tr$, is (in absolute value) much smaller than unity. By adopting this approximation, simple algebraic manipulations led to an expression relating the Sherwood number to the transpiration, flux, and Péclet numbers. The comparison of the approximate theory with CFD results (in which no such approximation was used) showed a good agreement provided the condition $Sc \cdot |Tr| \ll 1$ was met.

By using the above approximation, a complete map was drawn of the Sherwood number in the (Fl, Tr) plane for a given value of Pe. Different regions were identified, and the directions of the diffusive, convective and total solute flux (along with the shape of concentration profiles) associated with each region were highlighted. *Loci* of singularity, associated with Sh diverging to $\pm\infty$, occurred in correspondence with the line Fl=Tr, where the combined flux of solute and solvent through the walls is equivalent to the inflow or outflow of solution at the same concentration as that flowing in the channel.

Finally, using either the simplified theory or CFD simulations, profiles of the Sherwood number along the streamwise direction were obtained for different values of the flux and transpiration numbers. A noteworthy feature of these curves was that, unlike in channel flow with no transpiration, Sh did not settle to a fully developed value but varied along the channel also after entry effects vanished.

Acknowledgments

This work has been performed within the BAoBaB (Blue Acid/Base Battery) project, Horizon 2020 programme, Grant Agreement no. 731187, http://www.baobabproject.eu.

NOMENCLATURE

Symbol	Quantity	Unit
A	Cross sectional area	m^2
Cr	Concentration ratio C_{eq}/C_b	-
C	Concentration	- ($kg\ kg^{-1}$)
C_f	Fanning friction coefficient	-
D	Solute diffusivity	$m^2\ s^{-1}$
d_{eq}	Hydraulic diameter (=$4A/Pm$)	m
Fl	Flux number, $j_S/(\rho U C_b)$	-
Gz	Graetz number, $\mathrm{Pe}\cdot d_{eq}/x$	-
H	Channel thickness	m
j	Mass flux	$kg\ m^{-2}\ s^{-1}$
k	Mass transfer coefficient	$m\ s^{-1}$
L	Dimensionless duct length, $4l/d_{eq}$	-
l	Duct length	m
p	Pressure	Pa
Pe	Péclet number, Re·Pr or Re·Sc	-
P	Wet perimeter	m
Re	Reynolds number, $Ud_{eq}\rho/\mu$	-
Sc	Schmidt number, $\mu/(\rho D)$	-
Sh	Sherwood number, kd_{eq}/D	-
St	Stanton number, Nu/(Re·Pr) or Sh/(Re·Sc)	-
Tr	Transpiration number, $j_W/(\rho U)$	-
U	Cross-section-averaged velocity	$m\ s^{-1}$
U_∞	Free stream velocity	$m\ s^{-1}$
u_j	Generic velocity component	$m\ s^{-1}$
u	Velocity vector	$m\ s^{-1}$
v	Transpiration velocity	$m\ s^{-1}$
X	Dimensionless distance from inlet, $4x/d_{eq}$	-
x	Distance from inlet or leading edge	m
y	Coordinate orthogonal to the wall	m

Greek symbols

Δp	Pressure difference	Pa
$\Delta \pi$	Osmotic pressure difference	Pa
θ	Azimuthal coordinate in (Tr, Fl) plane	deg
μ	Solution viscosity	Pa s
π	Osmotic pressure	Pa
ρ	Solution density	kg m^{-3}
σ	Rejection coefficient	-

Subscripts/superscripts

b	Bulk
conv	Convective
diff	Diffusive
eq	Equivalent
i	Inlet
S	Solute
tr	Transpiration
W	Solvent
w	Wall
0	No-transpiration value

References

[1] W. M. Kays, R. J. Moffat, *The behaviour of transpired turbulent boundary layers*, Report No. HMT-20, Thermosciences Division, Department of Mechanical Engineering, Stanford University, Stanford, CA, April 1975.

[2] R. N. Meroney, *Laminar/turbulent transition in transpired boundary layers*, Final report, NSF Grant ENG-70-01360 (GK 23989), Fluid Dynamics and Diffusion Laboratory, College of Engineering, Colorado State University, Fort Collins, CO, December 1974.

[3] J. Polezhaev, The transpiration cooling for blades of high temperatures gas turbine, *Energy Convers. Mgmt* **38** (1997), 1123-1133.

[4] R. W. Newman, R. W. Allen, Compact transpiration cooling systems, *APL Technical Digest* (may-june 1972) 13-21.

[5] P. A. Marrone, M. Hodes, K. A. Smith, J. W. Tester, Salt precipitation and scale control in supercritical water oxidation—part B: commercial/full-scale applications, *J. Supercrit. Fluids* **29** (2004) 289–312.

[6] J. C. de la Rosa, L. E. Herranz, J. L. Muñoz-Cobo, Analysis of the suction effect on the mass transfer when using the heat and mass transfer analogy, *Nucl. Eng. and Design* **239** (2009) 2042–2055.

[7] T.-F. Zien, *Approximate analysis of heat transfer in transpired boundary layers at limiting Prandtl numbers*, Report No. AD-785 239, Naval Ordnance Laboratory, White Oak, MD, 1 July 1974.

[8] M. F. La Cerva, M. Di Liberto, L. Gurreri, A. Tamburini, A. Cipollina, G. Micale, M. Ciofalo, Coupling CFD with simplified 1-D models to predict the performance of Reverse Electrodialysis stacks, *J. of Membrane Sci.* **541** (2017) 596-610.

[9] A. Campione, L. Gurreri, M. Ciofalo, G. Micale, A. Tamburini, A. Cipollina, Electrodialysis for water desalination: a critical assessment of recent developments on process fundamentals, models and applications, *Desalination* **434** (2018) 121-160.

[10] S. S. Sablani, M. F. A. Goosen, R. Al-Belushi, M Wilf, Concentration polarization in ultrafiltration and reverse osmosis: a critical review, *Desalination* **141** (2001) 269-289.

[11] M. Amokrane, D. Sadaoui, C. P. Koutsou, A. J. Karabelas, M. Dudeck, A study of flow field and concentration polarization evolution in membrane channels witht wo-dimensional spacers during water desalination, *J. of Membrane Sci.* **477** (2015) 139–150.

[12] D. W. Green, R. H. Perry, *Perry's Chemical Engineers' Handbook*, 8th ed., McGraw-Hill, New York, 2007.

[13] M. Ciofalo, M. F. La Cerva, M. Di Liberto, A. Tamburini, Influence of the boundary conditions on heat or mass transfer in complex channels, *J. of Physics Conf. Ser.* **923** (2017), 012053.

[14] V. Gnielinski, *VDI-Wärmeatlas*, Springer-Verlag, Berlin, 1997.